# Synthesis and characterisation of $Sr_4Fe_{3-x}Cr_xO_{10-\delta}$

Jarvis, Abbey; Berry, Frank; marco, J; Sanchez-Arenillas, M; Sibin, G; Clemens, Oliver; Slater, Peter

*DOI:*
10.1016/j.jssc.2020.121372



*Document Version*
Peer reviewed version

*Citation for published version (Harvard):*
Jarvis, A, Berry, F, marco, J, Sanchez-Arenillas, M, Sibin, G, Clemens, O & Slater, P 2020, 'Synthesis and characterisation of $Sr_4Fe_{3-x}Cr_xO_{10-\delta}$: stabilisation of n=3 Ruddlesden-Popper phases through Cr doping', *Journal of Solid State Chemistry*, vol. 287, no. July, 121372. https://doi.org/10.1016/j.jssc.2020.121372

# Synthesis and characterisation of $Sr_4Fe_{3-x}Cr_xO_{10-\delta}$: stabilisation of n=3 Ruddlesden-Popper phases through Cr doping

A. Jarvis[a*], F.J. Berry[a], J. F. Marco[b], M. Sanchez-Arenillas[b], G. Cibin[c], O. Clemens[d,e], P. R. Slater[a*]

[a] School of Chemistry, University of Birmingham, Birmingham B15 2TT, UK
[b] Instituto de Química Física "Rocasolano", CSIC, Serrano 119, Madrid 28006, Spain
[c] Diamond Light Source, Limited, Didcot OX11 0DE, Oxfordshire, U.K.
[d] Materials Design by Synthesis, Technical University Darmstadt, Alarich-Weiss-Str. 2, 64287 Darmstadt, Germany
[e] Karlsruhe Institute of Technology, Institute of Nanotechnology, Hermann-von-Helmholtz Platz 1, 76344 Eggenstein-Leopoldshafen, Germany

[*]Correspondence to
Abbey Jarvis or Peter Slater
School of Chemistry
University of Birmingham
Birmingham
B15 2TT. UK

## Abstract

Ruddlesden-Popper type compounds have the general formula, $A_{n+1}M_nO_{3n+1\pm x}$ (typically A is a rare earth, alkaline earth, M is a transition metal), and are constructed of perovskite-type layers separated by rock salt type blocks. While n=1, 2 phases are typically straightforward to prepare, the synthesis of higher order (n>2) systems is difficult. In this paper we show that chromate ($CrO_4^{2-}$) doping can be exploited to stabilise new n=3 Ruddlesden-Popper systems, $Sr_4Fe_{3-x}Cr_xO_{10-\delta}$: without chromate doping, a mixture of the n=2 phase $Sr_3Fe_2O_{7-x}$ and perovskite-type $SrFeO_{3-x}$ is obtained. This can be explained by the stabilisation of the central perovskite building block by chromate incorporation, similar to prior work on sulfate and carbonate doping in this system. The structure, and Fe/Cr oxidation states were evaluated by X-ray diffraction, $^{57}$Fe Mössbauer spectroscopy and X-ray absorption spectroscopy supporting the incorporation of Cr as $CrO_4^{2-}$. In order to examine the potential of these new systems for use as a SOFC cathode material, conductivity studies were carried out, which showed semiconducting behaviour with slightly higher conductivities than the sulfate doped counterparts.

**Keywords:** solid oxide fuel cell; cathode; Ruddlesden-Popper; chromate

## 1. Introduction

Ruddlesden-Popper type compounds have the general formula $A_{n+1}B_nO_{3n+1}$, where typically A is an alkaline earth/rare earth element and B is a transition metal element. The structure consists of perovskite layers separated by rock salt layers where the number of perovskite layers increase as n increases. Ruddlesden-Popper materials have attracted interest as potential cathode materials for solid oxide fuel cells due to the flexible oxide ion defect characteristics: in particular, the structure is able to accommodate either oxide ion vacancies[1–8] (located in the perovskite-type layers) or oxide ion excess[5,9–12] (located in interstitial sites in the rock salt type layers). Most commonly investigated are the n=1 Ruddlesden-Popper systems, which are more commonly classified as materials with the $K_2NiF_4$ structure. In this respect, $La_2NiO_{4+\delta}$ has been widely studied as a cathode material for SOFCs.[5,13–16] Less widely studied are the n > 1 Ruddlesden-Popper systems, due to the more difficult synthesis of such systems, although $La_3Ni_2O_{7-\delta}$ and $La_4Ni_3O_{10-\delta}$ have been prepared and shown to display improved thermal stability, electrical conductivity and electrode performance compared to $La_2NiO_{4+\delta}$.[5] A key challenge for higher order (n>2) Ruddlesden-Popper phases is their synthesis. Thus for example, both $La_3Ni_2O_{7-\delta}$ and $La_4Ni_3O_{10-\delta}$ will decompose at elevated temperatures (typically above 1100°C) as oxygen loss leads to increased levels of oxide ion vacancies and hence instability in the structure. Similarly, while the n=2 Ruddlesden-Popper phase, $Sr_3Fe_2O_{7-x}$, is straightforward to synthesise, attempts to prepare the n=3 phase, $Sr_4Fe_3O_{10-x}$, in air produce a mixture of $Sr_3Fe_2O_{7-x}$ and perovskite-type $SrFeO_{3-x}$. This can be related to instabilities in the middle perovskite layer due to high oxide ion vacancy concentration. In prior work, we have shown that the introduction of oxyanion groups into perovskite systems can help to enhance the stability of phases containing large amounts of oxygen vacancies, which can be attributed to their lower coordination preference (tetrahedral (sulfate[17–21], phosphate[17,21–25], silicate[26–29]); trigonal planar (borate/carbonate[19,22,30–37])) which allocates the vacancies to the dopant itself. This can be further explained by the effect of this doping strategy on the perovskite tolerance factor. Hancock et al.[17,28] reported sulfate, phosphate and silicate doping in $SrCoO_3$ and silicate doping in $SrMnO_3$. Using Si doping of these materials as an example it can be expected that, assuming no change in oxygen content, the hexagonal perovskite would be obtained for both undoped and doped materials. This is due to the high tolerance factor (t>1) for $SrMnO_3$, which would be further increased by introduction of the smaller $Si^{4+}$, assuming no change in oxygen content. However, the critical point with these oxyanion dopants is that they adopt a lower coordination than 6, and so their inclusion requires either the presence or the creation of oxide ion vacancies. Thus Si incorporation leads to oxide ion vacancies in $SrMnO_3$ (replacement of octahedral $MnO_6^{8-}$ with tetrahedral $SiO_4^{4-}$). For charge balance, partial reduction of the remaining $Mn^{4+}$ occurs to give mixed valent $Mn^{4+}/Mn^{3+}$. The increased size of $Mn^{3+}$ outweighs the influence of the smaller $Si^{4+}$ leading to an overall reduction in the tolerance factor and the change to a cubic perovskite. Furthermore the mixed valency leads to an increase in electronic conductivity. Similar effects are seen for doping in $SrCoO_3$. Such doping approaches can be extended to Ruddlesden-Popper type compounds, with previous studies having shown sulfate[20,38] (Figure 1), carbonate[39] and combined sulfate/carbonate[40] incorporation into $Sr_4Fe_3O_{10-\delta}$, although in most cases, evacuated sealed tubes were required to allow the high temperature synthesis without loss of the oxyanion group. In these cases, the stabilisation of the n=3 Ruddlesden-Popper is attributed to the stabilisation of oxide ion vacancies around the oxyanion dopant. Given the potential of Cr to be incorporated as a $CrO_4^{2-}$ group, we illustrate here that this doping strategy can be similarly utilised to stabilise the n=3 member in air, and investigate the structures and conductivities of these doped systems.

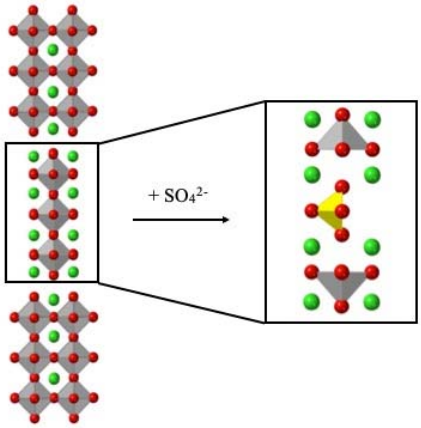


**Figure 1.** Structure of the n=3 Ruddlesden-Popper system, $Sr_4Fe_3O_{10-\delta}$, showing incorporation of $SO_4^{2-}$ in the middle perovskite layer. A single $SO_4^{2-}$ orientation is shown. A similar situation would be expected for $CrO_4^{2-}$ incorporation.

## 2. Experimental

The chromium doped $Sr_4Fe_{3-x}Cr_xO_{10-\delta}$ series (x=0.2 – 0.4) were prepared using stoichiometric amounts of $Cr_2O_3$, $SrCO_3$ and $Fe_2O_3$, which were intimately ground and heated to 950 °C for 12 h. Samples were then reground and heated to 1000 °C for 12 h, with a further regrinding and heat treatment to 1050 °C for 12 h in air. To ensure maximum oxygen content, samples were annealed at 350 °C for 12 h in air. Due to potential hazards associated with formation of $Cr^{6+}$ during the synthesis, all syntheses were performed in a furnace in a fumecupboard.

Powder X-ray diffraction (Panalytical Empyrean diffractometer equipped with a Pixcel 2D detector (Cu Kα radiation)) was utilised in order to determine phase purity and for subsequent structure refinement. Rietveld refinements (tetragonal space group, *I*4/*mmm*) were carried out using the GSAS suite of programs[41] on these Cr doped Ruddlesden-Popper samples. Lattice parameters and sample displacement parameters were refined for all samples. Due to anisotropic broadening in the XRD data, uniaxial strain models were included into the refinements. For all sites atom positions were refined, with oxygen occupancies additionally refined. Thermal parameters were constrained for Sr, Fe/Cr and O sites and fixed due to high correlation with site occupancies.

$^{57}$Fe Mössbauer spectra were recorded at 298 K in constant acceleration mode using an approximately 25 mCi Co/Rh source. The isomer shifts were referred to the centroid of the spectrum of metallic iron at room temperature.

Cr K-edge X-ray absorption spectroscopy (XAS) spectra were collected for $Sr_4Fe_{2.6}Cr_{0.4}O_{10-\delta}$, and standard materials, $LaCrO_3$ and $SrCrO_4$, on beamline B18 at Diamond Light Source (Rutherford Appleton Lab, Harwell, UK). Processing of data was performed using the Athena Software package.[42]

Thermogravimetric analysis (Netzch STA 449 F1 Jupiter Thermal Analyser with mass spectrometry attachment) were carried out under $N_2$ up to 1000 °C.

Pellets for 4 probe conductivity measurements were prepared by ball milling (350 rpm for 1 h, Fritsch Pulverisette 7 planetary mill) the samples, before then pressing into pellets. Pellets were then sintered at 1050 °C for 12 h after which four Pt electrodes were attached with Pt paste (and heated to 900 °C for 1 hr to ensure good contact) and finally annealed at 350 °C for 12 hr in air to ensure full oxygenation.

## 3. Results and Discussion

### 3.1 X-Ray Diffraction characterisation

The X-ray diffraction data showed that Cr doping was successful in allowing the synthesis of the n=3, $Sr_4Fe_{3-x}Cr_xO_{10-\delta}$, phase. Figure 2 shows the XRD data for x=0, 0.2, 0.25, 0.3, 0.35, 0.4 samples: without Cr doping (x=0), no n=3 phase is obtained, but rather a mixture of $Sr_3Fe_2O_{7-x}$ and $SrFeO_{3-x}$ is obtained. On Cr doping, the successful formation of the n=3 Ruddlesden-Popper phase, $Sr_4Fe_{3-x}Cr_xO_{10-\delta}$, is observed (Figure 2a). The stabilisation of the n=3 phase can be more clearly seen in the $2\theta$ range 40 to 60 ° (Figure 2b), where there is a clear difference in the diffraction data between the undoped and chromate doped phases. At higher Cr contents an extra impurity phase, $SrCrO_4$, is found in addition to the Ruddlesden-Popper type phase, indicating that the Cr solubility in the structure had been exceeded (Supplementary Information).

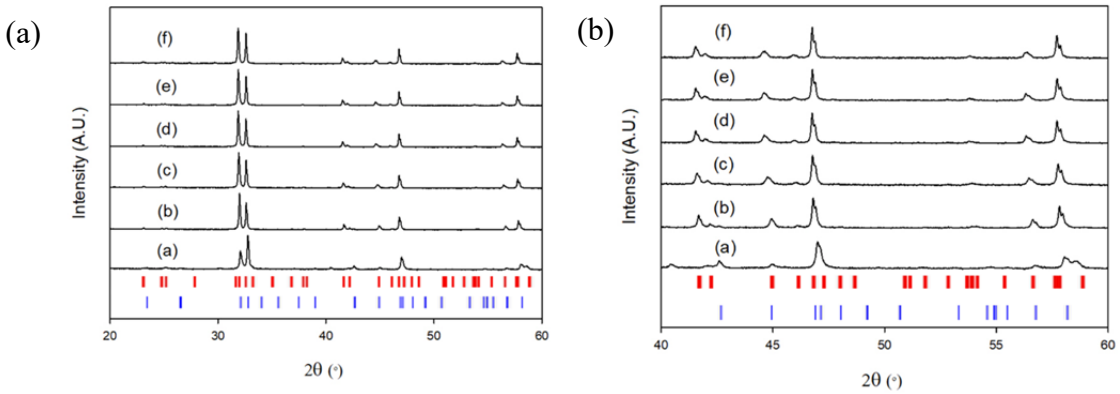


**Figure 2.** (a) X-ray diffraction patterns for $Sr_4Fe_{3-x}Cr_xO_{10-\delta}$ where a) x=0, b) x=0.2, c) x=0.25, d) x=0.3, e) x=0.35 and f) x=0.4. (b) Expanded region to illustrate differences between x = 0, and x > 0 samples. The two phases are indicated by red ($Sr_4Fe_{3-x}Cr_xO_{10-\delta}$, Ruddlesden-Popper n=3) and blue ticks ($Sr_3Fe_2O_{7-x}$, Ruddlesden-Popper n=2)

The structures of the resultant phases were evaluated through Rietveld refinement using the XRD data. Due to the X-ray scattering factors of chromium and iron being similar, the individual occupancy of these elements cannot be distinguished. Therefore the occupancy of all the transition metal (Fe/Cr) sites were set to 1. The refinements suggested the presence of a small amount of perovskite phase (≈ 3 - 7%), $Sr(Fe/Cr)O_{3-x}$, which was added as a second phase. Further improvements to the Rietveld refinement fits were achieved by including an anisotropic broadening model[43] to the refinements, suggesting the possibility of stacking faults within the structure (an example Rietveld fit is shown in Figure 3). The presence of

small perovskite impurities and stacking faults are common for higher order Ruddlesden-Popper systems.[44,45]

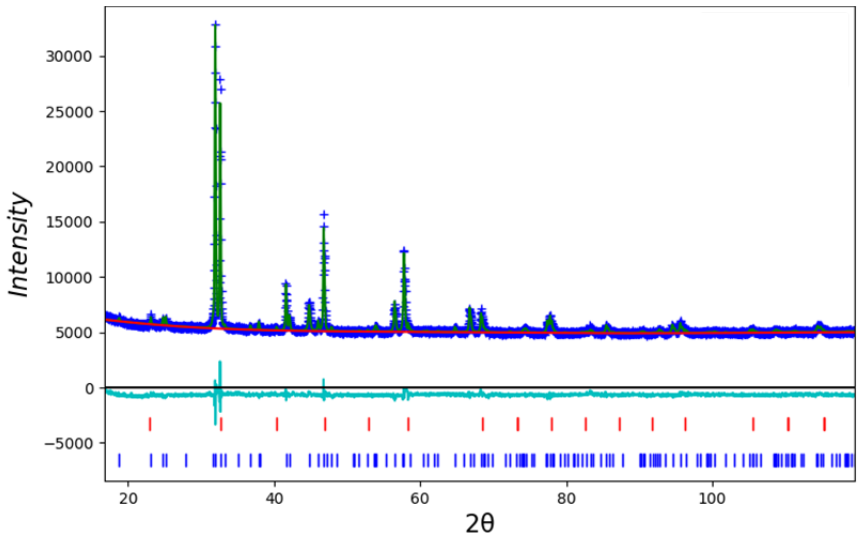


**Figure 3.** Observed, calculated and difference X-ray diffraction profiles for $Sr_4Fe_{2.75}Cr_{0.25}O_{10-\delta}$. The two phases are indicated by blue (Ruddlesden-Popper, *I*4/*mmm*) and red ticks (perovskite *Pm*-3*m*)

The final refined structural parameters are shown in Table 1. These data show an increase in unit cell parameters with increasing chromium content up to x=0.35 (Table 1, Figure 4). For x=0.35 and 0.4 a small additional impurity phase, $SrCrO_4$, was shown to also be present, supporting the conclusions from the cell parameter data, that the Cr doping limit is x<0.35.

**Table 1.** Lattice parameters, O occupancy and $U_{iso}$ values from Rietveld refinement of XRD data for $Sr_4Fe_{3-x}Cr_xO_{10-\delta}$. Ruddlesden-Popper, $Sr_4Fe_{3-x}Cr_xO_{10-\delta}$, was refined with space group *I*4/*mmm*. Additional impurities phases included Perovskite-type $Sr(Fe/Cr)O_{3-\delta}$ and $SrCrO_4$.

| | | $Sr_4Fe_{3-x}Cr_xO_{10-\delta}$ | | | | |
|---|---|---|---|---|---|---|
| Cr (x) | | 0.2 | 0.25 | 0.3 | 0.35 | 0.4 |
| a (Å) | | 3.8767(1) | 3.8791(1) | 3.8802(1) | 3.8805(1) | 3.8792(1) |
| c (Å) | | 28.2059(7) | 28.2919(9) | 28.3329(10) | 28.3541(8) | 28.3525(10) |
| V (Å$^3$) | | 423.91(2) | 425.72(3) | 426.58(3) | 426.97(3) | 426.66(3) |
| O occupancy | | 9.72 | 9.66 | 9.80 | 9.42 | 9.72 |
| $U_{iso}$ | Sr | 0.0163 | 0.0153 | 0.0141 | 0.0135 | 0.0128 |
| | Fe/Cr | 0.0026 | 0.00241 | 0.0017 | 0.0023 | 0.0020 |
| | O | 0.0405 | 0.0480 | 0.0473 | 0.0364 | 0.0495 |
| Rwp (%) | | 1.97 | 2.06 | 2.26 | 2.01 | 2.07 |
| Rexp (%) | | 1.33 | 1.33 | 1.35 | 1.36 | 1.36 |
| Perovskite ($SrFeO_3$) | a (Å) | 3.8672(3) | 3.8696(3) | 3.8702(3) | 3.8821(3) | 3.8812(2) |
| | V (Å$^3$) | 57.84(1) | 57.94(1) | 57.97(1) | 58.51(1) | 58.47(1) |
| Weight percentage (%) | Ruddlesden-Popper | 97.2 | 97.1 | 96.5 | 94.7 | 91.0 |
| | Perovskite | 2.8 | 2.9 | 3.5 | 3.8 | 6.3 |
| | $SrCrO_4$ | - | - | - | 1.5 | 2.7 |

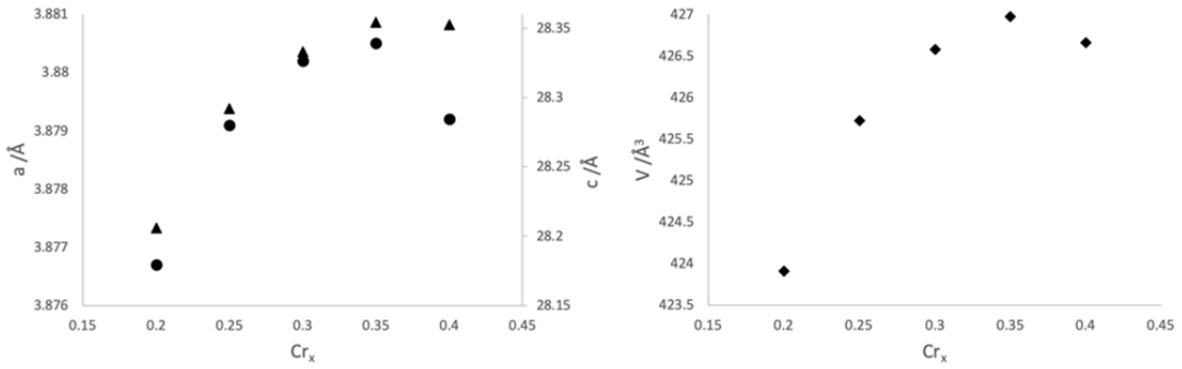


**Figure 4.** Variation of lattice parameters with Cr content (x) for $Sr_4Fe_{3-x}Cr_xO_{10-\delta}$, where a = ●, c =▲ and V = ◆. Error bars not included due to errors being smaller than the size of the data markers (errors given in Table 1)

### 3.2 X-ray absorption Spectroscopy (XAS)

The XRD data had indicated successful incorporation of Cr into the structure, but the oxidation state and coordination number needed further clarification. In order to evaluate this chromium environment/ oxidation state, XAS analysis was carried out on $Sr_4Fe_{2.6}Cr_{0.4}O_{10-\delta}$, and compared with data collected for $LaCrO_3$, $SrCrO_4$ and Cr foil standards. $LaCrO_3$ and $SrCrO_4$ were used as reference materials for octahedral $Cr^{3+}$ and tetrahedral $Cr^{6+}$ ($CrO_4^{2-}$) respectively, since previous studies have reported the presence of either $Cr^{3+}$ and $Cr^{6+}$ in Cr doped Ruddlesden-Popper systems. In particular, Sousa et al.[46] reported the presence of $Cr^{3+}$ and $Cr^{6+}$ in Cr doped $Ca_4Mn_3O_{10}$, whereas Bréad et al.[33] reported only $Cr^{3+}$ in the $Sr_4FeCrO_6CO_3$ Ruddlesden-Popper system.

The X-ray absorption near edge structure (XANES) data for $Sr_4Fe_{2.6}Cr_{0.4}O_{10-\delta}$ and the $LaCrO_3$ and $SrCrO_4$ standards are shown in Figure 5. The $SrCrO_4$ reference material is found to have a sharp pre edge at 5994 eV which correlates with tetrahedral chromium in the 6+ oxidation state. In comparison a weak pre edge is observed for $LaCrO_3$ which is characteristic of $Cr^{3+}$ in an octahedral coordination. The data for $Sr_4Fe_{2.6}Cr_{0.4}O_{10-\delta}$ are similar to $SrCrO_4$, with a similar sharp pre edge at 5994 eV. Therefore the XANES data support the original proposal that Cr is incorporated as $CrO_4^{2-}$ (tetrahedral $Cr^{6+}$).

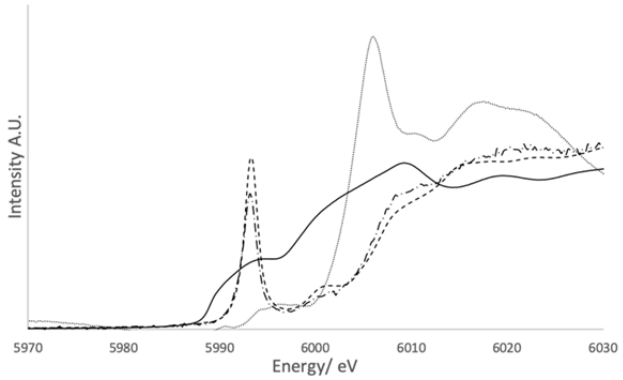


**Figure 5.** XANES data obtained for Cr foil ( ___ ), $LaCrO_3$ ( ..... ), $SrCrO_4$ ( - - - ) and $Sr_4Fe_{2.6}Cr_{0.4}O_{10-\delta}$ ( -.-. )

### 3.3 $^{57}$Fe Mössbauer Spectroscopy

In order to evaluate the Fe environment in these Ruddlesden Popper phases, $^{57}$Fe Mössbauer spectra were recorded from $Sr_4Fe_{2.8}Cr_{0.2}O_{10-\delta}$ and $Sr_4Fe_{2.6}Cr_{0.4}O_{10-\delta}$ (Figure 6). The spectra were fitted considering three different contributions. Their corresponding hyperfine parameters are collected in Table 2. These isomer shifts indicate that both these materials contain $Fe^{3+}$ and $Fe^{5+}$ with at least some of the $Fe^{3+}$ in lower than octahedral coordination. As reported for oxyanion doped perovskite and Ruddlesden-Popper systems,[20,27] disproportionation of $Fe^{4+}$ to $Fe^{3+}$ and $Fe^{5+}$ can be attributed to the substitution of smaller $Cr^{6+}$ for $Fe^{4+}$, with the disproportionation process allowing for the release of local strain. This, again, supports the incorporation of higher valence Cr (Figure 6).

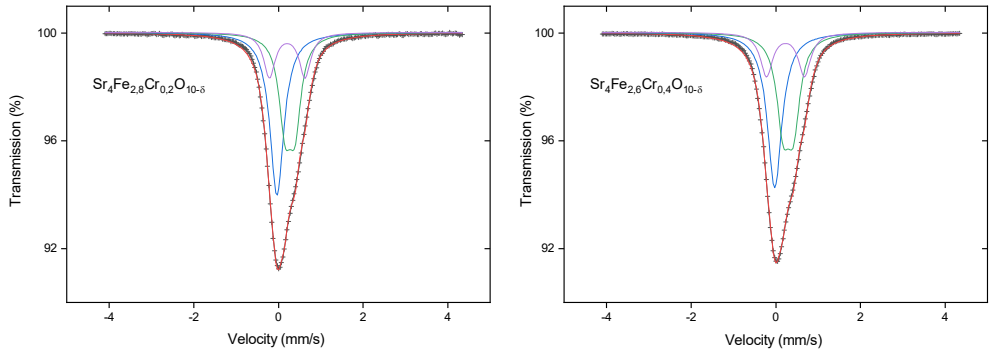


**Figure 6.** $^{57}$Fe Mössbauer spectra recorded from $Sr_4Fe_{2.8}Cr_{0.2}O_{10-\delta}$ and $Sr_4Fe_{2.6}Cr_{0.4}O_{10-\delta}$ at 298K

**Table 2.** $^{57}$Fe Mössbauer parameters recorded from $Sr_4Fe_{2.8}Cr_{0.2}O_{10-\delta}$ and $Sr_4Fe_{2.6}Cr_{0.4}O_{10-\delta}$ at 298K

| **Compound** | **Assignment** | **δ ± 0.01 (mms$^{-1}$)** | **Δ ± 0.05 (mms$^{-1}$)** | **Area ± 5%** |
|---|---|---|---|---|
| $Sr_4Fe_{2.8}Cr_{0.2}O_{10-\delta}$ | $Fe^{5+}$ | -0.04 | 0.00 | 43 |
| | $Fe^{3+}$ | 0.27 | 0.23 | 38 |
| | $Fe^{3+}$ in low coordination | 0.21 | 0.84 | 19 |
| $Sr_4Fe_{2.6}Cr_{0.4}O_{10-\delta}$ | $Fe^{5+}$ | -0.03 | 0.00 | 41 |
| | $Fe^{3+}$ | 0.30 | 0.24 | 40 |
| | $Fe^{3+}$ in low coordination | 0.23 | 0.90 | 19 |

### 3.4 Conductivity measurements

The data for all $Sr_4Fe_{3-x}Cr_xO_{10-\delta}$ samples show three linear regions (Figure 7) between 400 – 800 °C, which can be correlated with small changes in composition, and hence Fe oxidation states on heating as indicated by TGA studies. An initial increase in conductivity is observed with increasing temperature, indicative of the expected semiconducting behaviour. Above ≈ 640 - 670 °C a decrease in conductivity is observed which can be correlated with loss of oxygen at higher temperature which reduces the

average transition metal oxidation state, as shown in prior work for sulfate doping.[20] In addition to the loss of oxygen in the temperature range 400 – 800 °C, thermogravimetric analysis (TGA-MS) indicated some loss of water at ≈ 640 – 670 °C, suggesting a partial hydration of these systems. Deviations to the increase in conductivity are additionally observed at the lower temperature in the range ≈ 400 – 460 °C, which can be correlated to an additional loss of oxygen, and hence reduction in average Fe oxidation state, in this temperature range.

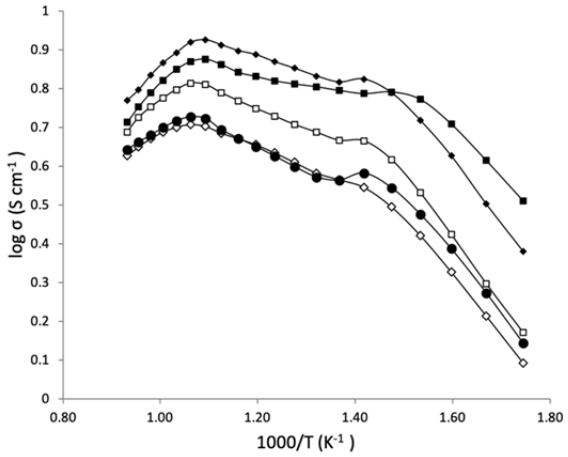


**Figure 7.** Plot of log σ vs. 1000/T for $Sr_4Fe_{2.8}Cr_{0.2}O_{10-\delta}$ (■), $Sr_4Fe_{2.75}Cr_{0.25}O_{10-\delta}$ (◆), $Sr_4Fe_{2.7}Cr_{0.3}O_{10-\delta}$ (□), $Sr_4Fe_{2.65}Cr_{0.35}O_{10-\delta}$ (◇) and $Sr_4Fe_{2.6}Cr_{0.4}O_{10-\delta}$ (●) in air

When comparing the conductivities of the present chromate doped samples, $Sr_4Fe_{3-x}Cr_xO_{10-\delta}$, to prior work on sulfate doped systems[20], slightly higher conductivities are observed at elevated temperatures for the former (Figure 8), although overall conductivities are still rather low (8.4 S $cm^{-1}$ at 642 °C for x=0.25) compared to common SOFC electrode materials.[47] Further doping studies, e.g. with Co, Cu, are planned to attempt to increase these values.

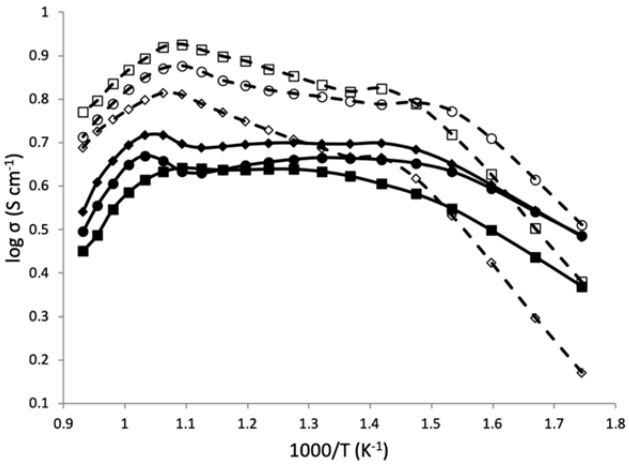


**Figure 8.** Plot of log σ vs. 1000/T for $Sr_4Fe_{2.8}S_{0.2}O_{10-\delta}$ (●), $Sr_4Fe_{2.75}S_{0.25}O_{10-\delta}$ (■), $Sr_4Fe_{2.7}S_{0.3}O_{10-\delta}$ (◆), $Sr_4Fe_{2.8}Cr_{0.2}O_{10-\delta}$ (○), $Sr_4Fe_{2.75}Cr_{0.25}O_{10-\delta}$ (□) and $Sr_4Fe_{2.7}Cr_{0.3}O_{10-\delta}$ (◇) in air (conductivity data for sulfate doped samples taken from reference[20])

### 3.5 Implications of Cr doping on the formation of $Sr_4Fe_3O_{10-x}$

Overall the results show that Cr doping in place of Fe can be utilised to allow the formation of the n=3 Ruddlesden Popper phase, $Sr_4Fe_3O_{10-y}$. The XANES results indicate that the oxidation state of Cr is 6+ and the coordination is tetrahedral, which is hence consistent with the incorporation as $CrO_4^{2-}$. Thus the $Cr_2O_3$ ($Cr^{3+}$) starting reagent has been oxidised during the synthesis to $Cr^{6+}$. This is not surprising given that $SrCrO_4$ is prepared similarly, and indeed also forms as an impurity phase when the Cr doping limit increases. The stabilisation of this n=3 Ruddlesden Popper phase by Cr doping can be attributed both to the high oxidation state and incorporation of tetrahedral $CrO_4^{2-}$. Undoped $Sr_4Fe_3O_{10-y}$ would be expected to have high levels of oxide ion deficiency (y) due to the high Fe oxidation otherwise needed (for y=0, all the Fe would be 4+). Such vacancies might be expected to concentrate in the middle perovskite layer, hence causing a structural instability here, which therefore favours phase separation to the n=2 ($Sr_3Fe_2O_{7-x}$) phase and perovskite-type $SrFeO_{3-x}$ as is observed in the XRD data for this system. The incorporation of Cr as $CrO_4^{2-}$ has two beneficial effects towards the stabilisation on the n=3 system; firstly the high oxidation state lowers the required Fe oxidation state from the parent system; secondly the incorporation as a tetrahedral unit leads to two stable vacancy positions around each $CrO_4^{2-}$ group (as discussed in the introduction for perovskite systems, an octahedral $FeO_6^{8-}$ group can be considered as being replaced by a tetrahedral $CrO_4^{2-}$ group and accompanying partial reduction of other Fe sites in the structure). Thus, it is most likely not just the high Cr oxidation state, but also its lower coordination number that is key to structural stabilisation, as is also the case for $CO_3^{2-}$, $SO_4^{2-}$ doping, which have been previously similarly shown to stabilise this higher order Ruddlesden Popper phase. The implication then is that we should consider both oxidation state and coordination preference when performing doping strategies in solid state materials.

## 4. Conclusions

In this work, we have shown for the first time that Cr doping can be utilised to allow the synthesis of the n=3 Ruddlesden-Popper system, $Sr_4Fe_3O_{10-\delta}$. XANES data indicate that Cr is incorporated as $CrO_4^{2-}$ (tetrahedral Cr(VI)). We believe that this is accommodated in the central perovskite layer, similar to sulfate, which helps to stabilise this central layer. In comparison to prior work on sulfate doped $Sr_4Fe_3O_{10-\delta}$ materials, improved conductivity is reported at higher temperatures, although further doping studies are required to try to increase the conductivities further, with a view to potential for use in SOFCs. Overall, the work illustrates the potential of doping strategies involving tetrahedral units in perovskite-related systems, with a view to stabilising new phases, and/or modifying the properties.

**CRediT authorship contribution statement**

**A. Jarvis:** Conceptualisation, Investigation, Formal analysis, Writing - original draft. **F.J. Berry:** Investigation, Writing - original draft, Formal analysis. **J.F. Marco:** Writing - original draft, Formal analysis. **M. Sanchez-Arenillas**: Writing - original draft, Formal analysis. **G. Cibin:** Writing - original draft, Formal analysis. **O.Clemens:** Writing - original draft, Formal analysis. **P.R. Slater:** Conceptualisation, Formal analysis, Writing -original draft.

**Declaration of competing interest**

The authors declare that they have no known competing financial interests or personal relationships that could have appeared to influence the work reported in this paper.

**Acknowledgements**

We would like to thank the University of Birmingham and EPSRC for funding (studentship for AJ). The authors also thank EPSRC for funding: the JUICED Hub (Joint University Industry Consortium for Energy (Materials) and Devices Hub), EP/R023662/1). We thank Diamond Light Source for the award of beam time as part of the Energy Materials Block Allocation Group. Financial support from the Spanish Ministry of Science and Innovation (project RTI2018-095303-B-51) is gratefully acknowledged.

Raw experimental data can be found at: https://doi.org/10.25500/edata.bham.00000442.

**Appendix A Supplementary data**

Supplementary data to this article can be found online at https://doi.org/10.1016/j.jssc.2020.121372.

**References**

1 D. Pelloquin, J. Hadermann, M. Giot, V. Caignaert, C. Michel, M. Hervieu and B. Raveau, *Chem. Mater.*, 2004, **16**, 1715–1724.
2 I. D. Fawcett, G. M. Veith, M. Greenblatt, M. Croft and I. Nowik, *J. Solid State Chem.*, 2000, **155**, 96–104.
3 G. Amow, J. Au and I. Davidson, *Solid State Ionics*, 2006, **177**, 1837–1841.
4 Y. Bréard, C. Michel, M. Hervieu, F. Studer, A. Maignan and B. B. Raveau, *Chem. Mater.*, 2002, **14**, 3128–3135.
5 G. Amow and S. J. Skinner, *J. Solid State Electrochem.*, 2006, **10**, 538–546.
6 T. Armstrong, F. Prado and A. Manthiram, *Solid State Ionics*, 2001, **140**, 89–96.
7 J. Y. Lee, J. S. Swinnea, H. Steinfink, W. M. Reiff, S. Pei and J. D. Jorgensen, *J. Solid State Chem.*, 1993, **103**, 1–15.
8 S. E. Dann and M. T. Weller, *J. Solid State Chem.*, 1995, **115**, 499–507.
9 H. Fjellvåg, O. H. Hansteen, B. C. Hauback and P. Fischer, *J. Mater. Chem.*, 2000, **10**, 749–754.
10 P. G. Radaelli, J. D. Jorgensen, A. J. Schultz, B. A. Hunter, J. L. Wagner, F. C. Chou and D. C. Johnston, *Phys. Rev. B*, 1993, **48**, 499–510.
11 K. Zheng and K. Świerczek, *Mater. Res. Bull.*, 2016, **84**, 259–266.
12 T. Broux, C. Prestipino, M. Bahout, O. Hernandez, D. Swain, S. Paofai, T. C. Hansen and C. Greaves, *Chem. Mater.*, 2013, **25**, 4053–4063.
13 B. Guan, W. Li, H. Zhang and X. Liu, *J. Electrochem. Soc.*, 2015, **162**, F707–F712.
14 S. J. Skinner and J. A. Kilner, *Solid State Ionics*, 2000, **135**, 709–712.
15 V. V Kharton, A. P. Viskup, E. N. Naumovich and F. M. B. Marques, *J. Mater. Chem.*, 1999, **9**, 2623–2629.
16 J. . Kilner and C. K. . Shaw, *Solid State Ionics*, 2002, **154**, 523–527.
17 C. A. Hancock, R. C. T. Slade, J. R. Varcoe and P. R. Slater, *J. Solid State Chem.*, 2011, **184**, 2972–2977.
18 Y. Liu, X. Zhu and W. Yang, *J. Memb. Sci.*, 2016, **501**, 53–59.
19 A. Jarvis and P. R. Slater, *Crystals*, 2017, **7**, 169–181.
20 A. Jarvis, F. J. Berry, J. F. Marco and P. R. Slater, *ECS Trans.*, 2019, **91**, 1467–1476.
21 J. F. Shin, A. Orera, D. C. Apperley and P. R. Slater, *J. Mater. Chem.*, 2011, **21**, 874–879.

22 J. M. Porras-Vazquez, T. F. Kemp, J. V. Hanna and P. R. Slater, *J. Mater. Chem.*, 2012, **22**, 8287–8293.
23 J. F. Shin, L. Hussey, A. Orera and P. R. Slater, *Chem. Commun.*, 2010, **46**, 4613–4615.
24 M. Li, W. Zhou, X. Xu and Z. Zhu, *J. Mater. Chem. A*, 2013, **1**, 13632–13639.
25 Y. Zhu, W. Zhou, J. Sunarso, Y. Zhong and Z. Shao, *Adv. Funct. Mater.*, 2016, **26**, 5862–5872.
26 J. M. Porras-Vazquez, R. I. Smith and P. R. Slater, *J. Solid State Chem.*, 2014, **213**, 132–137.
27 J. M. Porras-Vazquez, T. Pike, C. A. Hancock, J. F. Marco, F. J. Berry and P. R. Slater, *J. Mater. Chem. A*, 2013, **1**, 11834–11841.
28 C. A. Hancock and P. R. Slater, *Dalton Trans.*, 2011, **40**, 5599–5603.
29 J. F. Shin, D. C. Apperley and P. R. Slater, *Chem. Mater.*, 2010, **22**, 5945–5948.
30 J. M. Porras-Vazquez and P. R. Slater, *J. Power Sources*, 2012, **209**, 180–183.
31 J. Deakin, I. Trussov, A. Gibbs, E. Kendrick and P. R. Slater, *Dalt. Trans.*, 2018, **47**, 12901–12906.
32 B. Raveau, M. Hervieu, D. Pelloquin, C. Michel and R. Retoux, *Zeitschrift fur Anorg. und Allg. Chemie*, 2005, **631**, 1831–1839.
33 Y. Bréard, C. Michel, M. Hervieu, A. Ducouret, N. Nguyen, F. Studer, A. Maignan, B. Raveau and E. Suard, *Chem. Mater.*, 2001, **13**, 2423–2429.
34 Y. Bréard, C. Michel, M. Hervieu, N. Nguyen, F. Studer, A. Maignan, B. Raveau and F. Bourée, *J. Solid State Chem.*, 2003, **170**, 424–434.
35 Y. Bréard, C. Michel, A. Maignan, F. Studer and B. Raveau, *Chem. Mater.*, 2003, **15**, 1273–1282.
36 A. Demont, D. Pelloquin, S. Hébert, Y. Bréard, J. Höwing, Y. Miyazaki and A. Maignan, *J. Solid State Chem.*, 2011, **184**, 1655–1660.
37 A. J. McSloy, I. Trussov, A. Jarvis, D. J. Cooke, P. R. Slater and P. M. Panchmatia, *J. Phys. Chem. C*, 2018, **122**, 1061–1069.
38 B. Gonano, Y. Bréard, D. Pelloquin, V. Caignaert, O. Perez, A. Pautrat, P. Boullay, P. Bazin and J. M. Le Breton, *Inorg. Chem.*, 2017, **56**, 15241–15250.
39 K. Yamaura, Q. Huang, J. W. Lynn, R. W. Erwin and R. J. Cava, *J. Solid State Chem.*, 2000, **152**, 374–380.
40 B. Gonano, Y. Bréard, D. Pelloquin, V. Caignaert, O. Pérez, A. Pautrat, P. Bazin, E. Suard and P. Boullay, *Dalt. Trans.*, 2018, **47**, 13088–13093.
41 B. H. Toby and R. B. Von Dreele, *J. Appl. Crystallogr.*, 2013, **46**, 544–549.
42 B. Ravel and M. Newville, *J. Synchrotron Radiat.*, 2005, **12**, 537–541.
43 P. W. Stephens, *J. Appl. Crystallogr.*, 1999, **32**, 281–289.
44 R. Seshadri, M. Hervieu, C. Martin, A. Maignan, B. Domenges, B. Raveau and A. N. Fitch, *Chem. Mater.*, 1997, **9**, 1778–1787.
45 J. Grins, D. Wardecki, K. Jansson, S. Carlson, J. J. Biendicho and G. Svensson, *J. Mater. Chem. A*, 2018, **6**, 5313–5323.
46 P. M. Sousa, A. V. Girão, M. E. M. Jorge, M. D. Carvalho, P. M. Costa, R. P. Borges, M. M. Cruz and M. Godinho, *J. Phys. Chem. Solids*, 2004, **65**, 1823–1829.
47 A. Orera and P. R. Slater, *Chem. Mater.*, 2010, **22**, 675–690.